Selective oxidation of glucose to gluconic acid and glucaric acid with chlorin e6 modified carbon nitride as metal-free photocatalyst

Xinyu Bai [a,1], Qidong Hou [a,*,1], Hengli Qian [a], Yifan Nie [a], Tianliang Xia [a], Ruite Lai [a], Guanjie Yu [a], Mian Laiq Ur Rehman [a], Haijiao Xie [b], Meiting Ju [a,*]

[a] National & Local Joint Engineering Research Center of Biomass Resource Utilization, College of Environmental Science and Engineering, Nankai University, Tianjin 300350, China
[b] Hangzhou Yanqu Information Technology Co., Ltd, Hangzhou City, Zhejiang Province, 310003, China

ARTICLE INFO

ABSTRACT

Photocatalysis has exhibited huge potential in many reactions, but the design of metal-free photocatalytic material for selective upgrading of biomass is rarely achieved. Here, we report that the metal-free photocatalyst consisted of nitrogen-deficient carbon nitride (BNCN) and chlorin e6 (Ce6) can efficiently and selectively oxidize glucose into gluconic acid and glucaric acid. Introducing nitrogen defects could significantly enhance the optical absorption and modulate the band structure. In addition, the combination of Ce6 with BNCN further improve the optical absorption property and promote effective separation of photon-generated carriers. As expected, the resultant Ce6@BNCN catalyst gave a total selectivity of gluconic acid, glucaric acid and arabinose as high as 70.9% at glucose conversion up to 62.3%, as is superior to previously reported photocatalytic systems. The mechanism for the enhancement of catalytic performance and the reaction pathway were revealed by experimental studies combined with DFT calculations.

1. Introduction

The concerns on environmental problems have prompted the rapid development of biorefinery technologies which aim to transform cheap biomass resource into alternative chemicals and fuels [1–7]. As the most abundant monosaccharide from biomass, glucose upgrading toward various products has attracted increasing attentions [8–13]. Particularly, catalytic oxidation of glucose could deliver a variety of valuable chemicals [11–16], such as gluconic acid [17–19], glucaric acid [10,16, 20,21] and arabinose [22–25]. Thus, establishing effective catalytic system for glucose upgrading to these products is highly desirable.

Currently, industrial production of gluconic acid is based on glucose oxidation by costly enzymes [26]. The production of glucaric acid requires the use of toxic nitric acid or bleaching agents as oxidant, generating intractable wastes [27–30]. Precious metals have also been extensively tested for this process, but their practical applications are impeded by low selectivity, large energy consumption and high cost [31]. Recently, photocatalysis technology which could use solar energy to drive oxidation process has been increasingly studied, as a promising

alternative to traditional technologies [25,26,31–37]. In this context, photocatalytic oxidation using various semiconductor materials, such as TiO_2, C_3N_4 and CdS are on the rise [38–41]. However, the photocatalytic conversion of glucose universally gives low selectivity of desirable products, indicating semiconductor materials alone are not suitable catalyst for selective oxidation [42]. On one hand, the reactive oxygen species with strong oxidizing power generally promote overoxidation and/or complete mineralization of organic compounds [31,43]. On the other hand, selectively oxidizing glucose at target position is tough due to the presence of multiple fragile functional groups [43].

Compared with semiconductor materials, several molecular photocatalysts are proved to be capable to selectively generate reactive oxygen species with controllable oxidizing power, thus achieving high selectivity in oxidation reactions. For example, Xu et al. reported that cobalt thioporphyrazine (CoPz) could selectively oxidize 5-hydroxymethylfurfural, affording high selectivity of 2,5-furandicarboxylic acid albeit at moderate conversion [31]. Moreover, the loading of CoPz onto g-C_3N_4 could greatly improve the stability of catalyst and then afford high yield with good selectivity. Similarly, Zhang et al. showed that

combining iron thioporphyrazine with SnO_2 enables glucose oxidation toward gluconic acid, glucaric acid and formic acid, affording total organic acids selectivity of 52.2% at conversion of 34.2% [32]. They showed that the combination of g-C_3N_4 with cobalt tetra(2,3-bis (butylthio)maleonitrile)porphyrazine) could also drive this reaction [26]. As proof of concept, these works have demonstrated the superiority of composite photocatalyst in the elegant regulation of oxidative ability and reaction pathway. However, the metal-containing molecular catalysts generally require complicated synthesis, separation and purification processes. Meanwhile, the secondary contaminations associated with metal ion leakage need to be solved [44]. Moreover, the fundamental understanding on the role of semiconductor material and molecular catalyst in photocatalytic oxidation process as well as their interactions in composite material are still limited.

Inspiring by the development of highly effective composite photocatalyst composed of semiconductor materials and metal-containing molecular catalysts, in the present study we aim to construct high-performance, metal-free composite photocatalyst by integrating Chlorin e6 (Ce6) with carbon nitride materials. The results of material synthesis and characterization indicated that the composite of nitrogen-deficient carbon nitride and Ce6 exhibited a series of advantages, such as better optical absorption property and higher separation efficiency of photon-generated carriers than Ce6 and carbon nitride materials. Moreover, the catalyst gives a total selectivity of gluconic acid, glucaric acid and arabinose as high as 70.9% at glucose conversion up to 62.3%, exceeding most of photocatalysts. The reaction pathway and mechanism was investigted by combined experimental studies and DFT calculations.

2. Experimental

2.1. Materials and reagents

Melamine (CH_4N_2O, 99.9%, Aladdin), glucose ($C_6H_{12}O_6$, 98%, Bide Pharmatech Ltd.), hydrogen peroxide (H_2O_2, 30%, Yinuokai), sodium carbonate (Na_2CO_3, 99.8%, Heowns), sodium borohydride ($NaBH_4$, 98%, Fuchen), hydrochloric acid (HCl, 36–38%, Heowns), isopropanol (C_3H_8O, 99.5%, Aladdin), β-Carotene ($C_{40}H_{56}$, 96%, Heowns), p-benzoquinone (BQ, 98%, Heowns), potassium iodide (KI, 98%, Heowns) and chlorin e6 (Ce6, 94%, Macklin) were used directly without further purification.

2.2. Material synthesis

Pristine g-C_3N_4 was obtained by thermal polymerization of melamine in alumina crucible with a cover at 520ºC in air for 4 h with a ramping rate of 5ºC/min [45,46]. g-C_3N_4 was then treated with $NaBH_4$ under N_2, according to previously reported method with slight modification [47]. Briefly, 0.4 g of as-prepared g-C_3N_4 and 0.16 g of $NaBH_4$ were milled finely and then calcined at 400ºC in nitrogen flow for 1 h. The obtained products were washed with ethanol and deionized water alternately to remove unreacted $NaBH_4$ and then dried under vacuum at 80ºC for 10 h. The final product was named as BNCN.

The protonation of as-prepared BNCN was conducted with hydrochloric acid solution under magnetic stirring for 5 h, to regulate the surface charge features [48]. After washing and drying, protonated BNCN was denoted as pBNCN. Protonated g-C_3N_4 (pCN) is prepared from pristine g-C_3N_4 via the same process.

To achieve the combination of Ce6 with BNCN, 0.5 g of pBNCN was added to 100 mL of water, followed by addition of 0.05 g of Ce6, and then stirred for 2 h. Afterwards, the solid product (denoted as Ce6@BNCN) was purified by washing and dried under vacuum at 80 °C overnight. As a control sample, Ce6@g-C_3N_4 was prepared by displacing pBNCN with same amount of pCN.

2.3. Catalyst characterization

The morphology of the samples was observed by transmission electron microscopy (TEM, Talos F200X G2 electron microscope operating at 200 kV) and scanning electron microscopy (SEM, JSM-7800 F electron microscope operating at 0.01~30 kV). The FTIR spectra (Tensor 37) were determined to characterize the functional groups of catalyst. X-ray powder diffraction (XRD, 40 kV and 40 mA) patterns were used to characterize the crystalline structure. Fluorescent images were recorded on confocal laser scanning microscopy (Zeiss; excitation: 405/488 nm; emission: 465/630). The N_2 adsorption-desorption isotherms was used to analyze the channel structure of samples. The X-ray photoelectron spectroscopy (XPS) was recorded on a Thermo ESCALAB 250XI. The optical properties of catalysts were examined with an ultraviolet-visible diffuse reflectance spectrometer (UV–vis DRS; UV-3600, Shimazu) and a photoluminescence fluorescence spectrometer (PL; FLS9800, Edinburgh instruments), respectively.

2.4. Oxidation of glucose via photocatalysis

The reaction was carried out in a 100 mL cylindrical vessel which is equipped with a circling water to control the reaction temperature (25 °C), using A 300 W xenon lamp (PLSSXE300DUV, Beijing Perfect-light). 30 mL of glucose aqueous solution (1 mmol/L) was added into the reactor with 10 mg of catalyst. Prior to the initiation of photocatalytic reaction, the reaction mixture was stirred under dark for 30 min to reach the equilibrium of adsorption and desorption. Afterwards, 30 μL of 30% aqueous H_2O_2 solution was added as oxidant, and then the reaction was started by radiation with xenon lamp with magnetic stirring.

The sample was tested on a Dionex Ultimate 3000 HPLC system using a HyperREZ XP Carbohydrate H^+ (7.7 mm × 300 mm) column and refractive index (RI) (ERC RefractoMax521) detector to separate and detect the main products. The mobile phase was 0.24 mmol·L^{-1} H_2SO_4 solution with flow rate of 0.6 mL·min^{-1}. The separation was performed at 65 °C and the injection volume was 100 μL. Liquid chromatography-mass spectrometry (LC-MS) analysis was conducted on a thermo scientific Q Exactive mass spectrometer.

2.5. Density functional theory calculations

All of spin-polarized calculations according to density functional theory (DFT) were performed by utilizing DMol3 package [49]. The generalized gradient approximation (GGA) in the Perdew–Burke–Ernzerhof form and Semicore Pseudopotential method (DSPP) with the double numerical basis sets plus the polarization functional (DNP) were adopted [50,51]. A DFT-D correction with Grimme scheme was used to account for the dispersion interaction [52]. The SCF convergence for each electronic energy was appointed as 1.0×10^{-5} Ha. The geometry optimization convergence criteria were appointed as follows: 1.0×10^{-5} Ha for energy, 0.004 Ha $Å^{-1}$ for force, and 0.01 Å for displacement, respectively. Energy barriers were tested by linear and quadratic synchronous transit methods combined with the conjugated gradient (CG) refinement.

3. Results and discussion

3.1. Catalyst synthesis and characterization

As shown in Fig. 1a, BNCN was synthesized by treating g-C_3N_4 with $NaBH_4$ at 400ºC for 1 h, and BNCN was first protonated by hydrochloric acid and then assembled with Ce6 to synthesize Ce6@BNCN. SEM and TEM images indicated that g-C_3N_4, BNCN and Ce6@BNCN composite are composed of sheet structures. The darker part in the TEM images was attributed to the overlap of several sheets [53,54]. Compared with g-C_3N_4, more wrinkles were observed on BNCN and Ce6@BNCN. To ascertain the formation of Ce6@BNCN composite, the element mapping
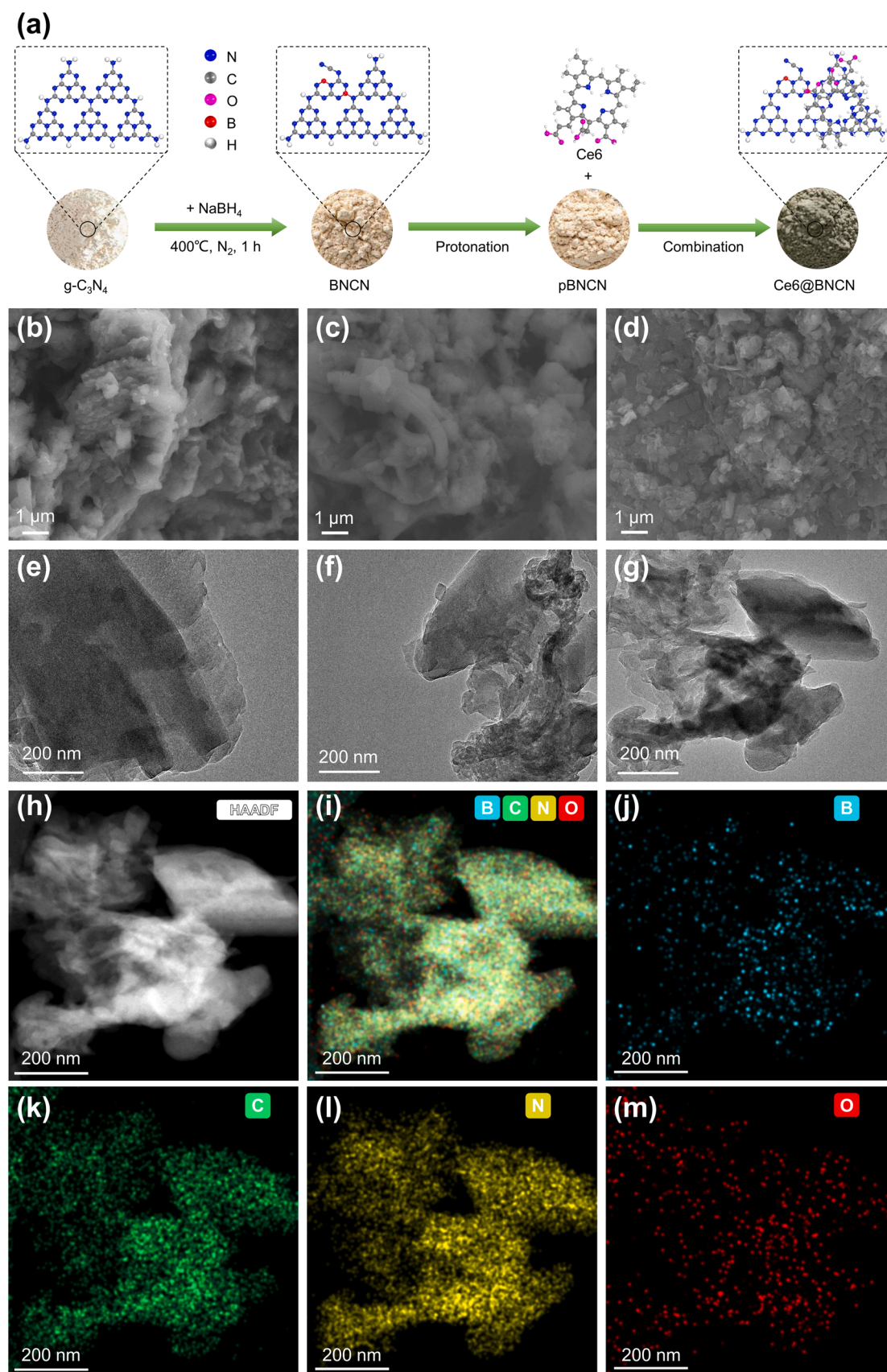
Fig. 1. (a) Synthesis process of Ce6@BNCN composite; SEM images of g-C₃N₄ (b), BNCN (c) and Ce6@BNCN (d); TEM images of g-C₃N₄ (e), BNCN (f) and Ce6@BNCN (g); STEM-EDS mapping images of Ce6@BNCN composite (h-m).

images of Ce6@BNCN composite were recorded. C, N, O and B elements were distributed evenly in Ce6@BNCN composite (Fig. 1j–m), suggesting that Ce6 are successfully loaded onto the surface of BNCN. The XRD patterns (Fig. S2) of g-C$_3$N$_4$ based materials had two pronounced peaks of the (002) and (100) planes of g-C$_3$N$_4$ [44,55,56]. Ce6@pCN and Ce6@BNCN contained diffraction peaks resulted from both Ce6 and the corresponding support materials, confirming that Ce6 has been successfully loaded onto the support.

The N$_2$ adsorption-desorption isotherms of five catalysts (Fig. S4a and b.) were type IV isotherm bearing H3 hysteresis loop [57,58], manifesting that all these materials have typical mesoporous structure. The hysteresis loop scope amplified from $P/P_0 = 0.70$–0.98 for BNCN to 0.45–0.98 for pBNCN, suggesting that the formation of small in-plane micropores. The five samples (Fig. S4b) all show main peak corresponding to micropores of 1.5–1.8 nm. pBNCN and Ce6@BNCN have slightly higher specific surface area (Table S1) than g-C$_3$N$_4$, indicating the in-plane micropores are well maintained after the loading with Ce6.

Except for Ce6, all the materials displayed FTIR peaks (Fig. 2a) similar with g-C$_3$N$_4$. The peak at 810 cm^{-1} was resulted from the breathing mode of triazine units [59]. The broad band between 1200 and 1700 cm^{-1} was assignable to the stretching modes of CN heterocycles, whereas the broad bands at 3000 and 3500 cm^{-1} were due to the

overlap of N-H stretching vibration and the O-H stretching mode [60, 61]. Compared with g-C$_3$N$_4$, the strength of the N-H stretching peaks in BNCN decreased obviously with the appearance of a new peak (2180 cm^{-1}) attributed to the asymmetric stretching vibration of N≡C- groups [62]. These results indicate that treating g-C$_3$N$_4$ with NaBH$_4$ via thermal reaction decreases the concentration of -NH$_2$ groups while increases the concentration of N≡C- groups, forming reduced -NH$_2$ and introduced N≡C- as two kinds of nitrogen defects in the BNCN material, as is in accordance with previous reports [63].

The XPS survey spectra revealed that g-C$_3$N$_4$, BNCN and Ce6@BNCN (Fig. 2b) are predominantly consisted of C, N and O elements. Specifically, the C 1s spectra (Fig. 2c) was divided into two peaks at 284.8 and 288.1 eV, corresponding to graphitic C and N═C(-N)$_2$, respectively [64]. Notably, the intensity of N and O containing species in Ce6@BNCN is considerably higher than that in BNCN, as is in accordance with FTIR analysis. The N 1s spectra (Fig. 2d) are divided into three peaks at 398.4, 399.7 and 401.1 eV (weak), resulting from C-N═C, N-(C)$_3$ and C-N-H, respectively [65,66]. The tertiary nitrogen N-(C)$_3$ peak in BNCN showed a binding energy lower than that of g-C$_3$N$_4$, owing to generation of nitrogen defects [67]. The O 1s peak (Fig. 2e) in g-C$_3$N$_4$ and BNCN was divided into three peaks centered at 531.1, 532.1 and 533.2 eV, assigned to O-C═O, N-C═O and C═O, respectively [68,69]. The C═O peak for
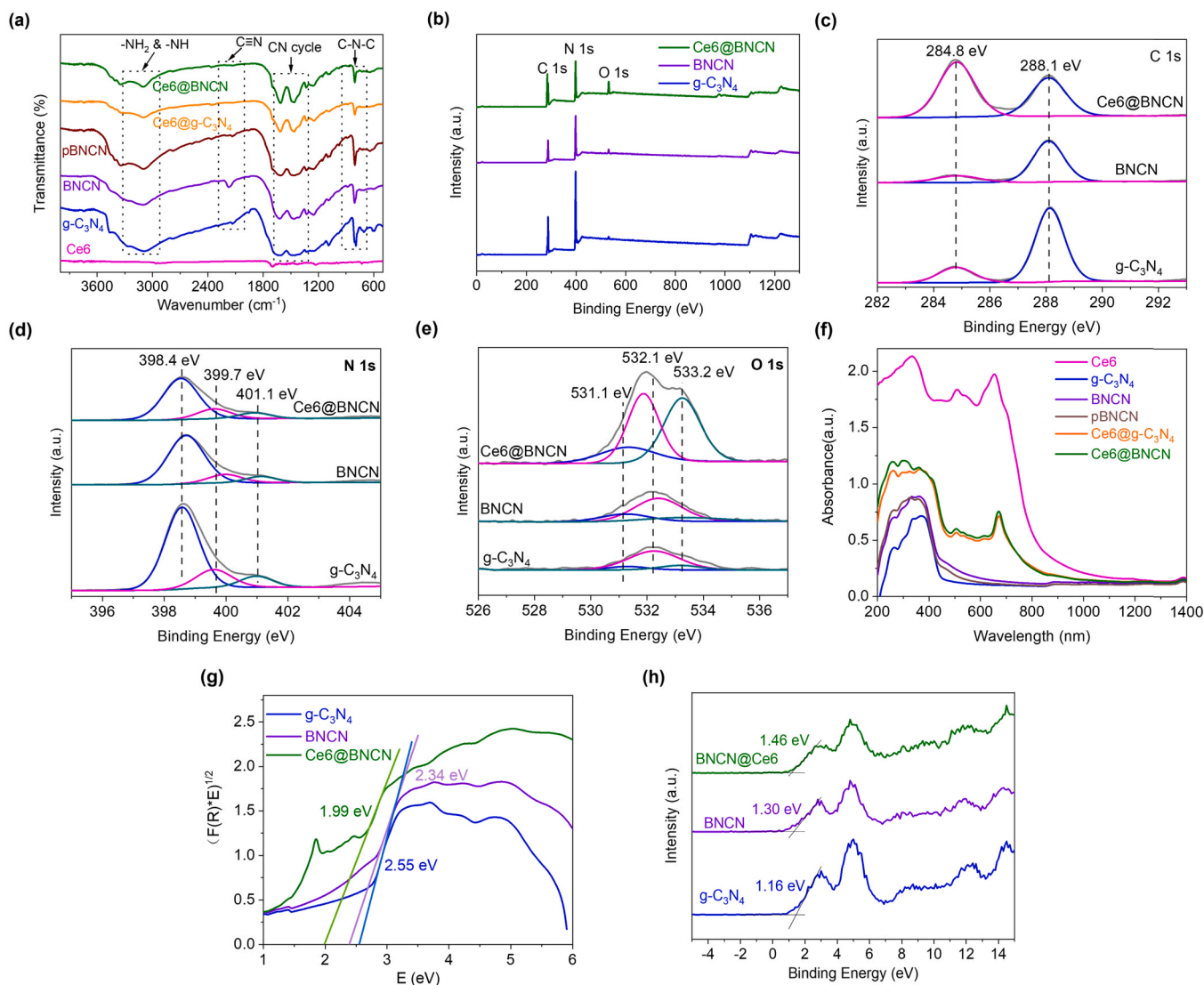
Fig. 2. (a) FTIR spectra; (b) XPS survey spectra and (c) C 1s peaks, (d) N 1s peaks and (e) O 1s peaks; (f) UV–vis absorption spectra; (g) estimated band gap curves; (h) XPS valence band.

Ce6@BNCN is considerably higher than BNCN owing to abundant carboxyl groups in Ce6 [44,55,56]. Meanwhile, the N-C=O peak shifted to lower binding energy with enhanced intensity, probably owing to the interaction between BNCN and Ce6.

The optical properties of Ce6@BNCN were examined. As a representative near-infrared (NIR) photosensitizer, Ce6 showed strong absorption in both UV and NIR region (Fig. 2f), while g-C$_3$N$_4$ just exhibited finite absorption in visible region [70,71]. In comparison with g-C$_3$N$_4$, the absorption edge of BNCN exhibited remarkable redshift with the appearance of sample changing from yellow to brown. At the same time, the bandgap greatly narrowed from 2.55 to 2.34 eV, and the VB maximum (Fig. 2h) improved from 1.16 to 1.30 eV. These results indicated that treating g-C$_3$N$_4$ with NaBH$_4$ not only remarkably improve the optical absorption but also modulate the band structures. When Ce6 was loaded onto g-C$_3$N$_4$ and BNCN, respectively, significant red-shift of optical absorption edges of Ce6@g-C$_3$N$_4$ and Ce6@BNCN both occurred in relative to the support materials, demonstrating that the coupling of Ce6 with BNCN can significantly enhance the energy harvesting in solar spectrum. One characteristic absorption peak of Ce6 shifted from 670 to 680 nm in Ce6@BNCN while the other characteristic absorption peak shifted from 330 to 300 nm, confirming the intimate interfacial interaction between Ce6 and BNCN [44,55,56]. On the whole, the band gap (1.99 eV) of Ce6@BNCN was narrower than those (2.55, 2.34 eV) of g-C$_3$N$_4$ and BNCN. The fluorescence microscopy of Ce6@BNCN further demonstrated that Ce6 has been successfully loaded onto the BNCN supports (Supporting Information, Fig. S3).

3.2. Photocatalytic conversion of glucose

Without any catalyst, a glucose conversion up to 88.8% (Fig. 3a) was achieved with H$_2$O$_2$ after 2 h reaction. However, the total selectivity of value-added products, including gluconic acid, glucaric acid and arabinose was just 31.7%. When using Ce6 as catalyst, the total selectivity reached as high as 94.8% at conversion of 11.6%, suggesting that the photosensitizer Ce6 is beneficial to the improvement of the selectivity of value-added products. Compared with g-C$_3$N$_4$, BNCN exhibited both

higher yield and selectivity. Among the tested materials, Ce6@BNCN composite was identified as the most effective and selective catalyst. The total selectivity is as high as 70.9% with glucose conversion up to 62.3%. The reaction didn't proceed in the presence of Ce6@BNCN composite under dark (Fig. S6), confirming that the selective oxidation of glucose is mainly driven by photocatalytic process.

The impact of initial concentration on the reaction are presented in Fig. 3b. It was observed that glucose conversion decreases gradually from 62.3% to 10.7% as glucose loading was boosted from 1 to 7 mmol·L^{-1}. As shown in Fig. 3c, the total selectivity is relatively low despite at high glucose conversion when the amount of catalyst is low (5 mg), akin to the result obtained with H$_2$O$_2$ in the absence of catalyst. It's notable that the increase of catalyst amount to 10 mg leads to remarkable improvement of products selectivity with slight reduction of glucose conversion. The further addition of catalyst dosage to 30 mg resulted in obvious enhancement of glucose conversion, as expected. In contrast, the selectivity displayed a downtrend when the catalyst amount is above 10 mg. Overall, the optimal amount of catalyst is 10 mg.

A remarkable improvement of glucose conversion was observed with the addition of H$_2$O$_2$ loading (Fig. 3d). The total selectivity of oxidation products reached the maximum when the H$_2$O$_2$ loading is 30 μL. The glucose conversion at H$_2$O$_2$ loading of 40 μL increased slightly in comparison with that at H$_2$O$_2$ loading of 30 μL, but the selectivity of oxidation products is obviously lower than the latter. Besides, the influences of acid and base on the reaction were investigated. Both acid and base lead to the reduction of yield (Supporting Information, Figs. S7 and S8).

The stability of Ce6@BNCN catalyst was investigated by five run's recycling experiment. As shown in Fig. 3e, the glucose conversion at the 5th run decreased by just 7.5%, compared with the first run. Moreover, the selectivity is almost kept except for the small fluctuation at the third run. The FT-IR spectra of recovered catalyst was tested, also confirming that the catalyst is stable during the recycling experiment (Supporting Information, Fig. S9).

We also compared the catalytic performance of the Ce6@BNCN
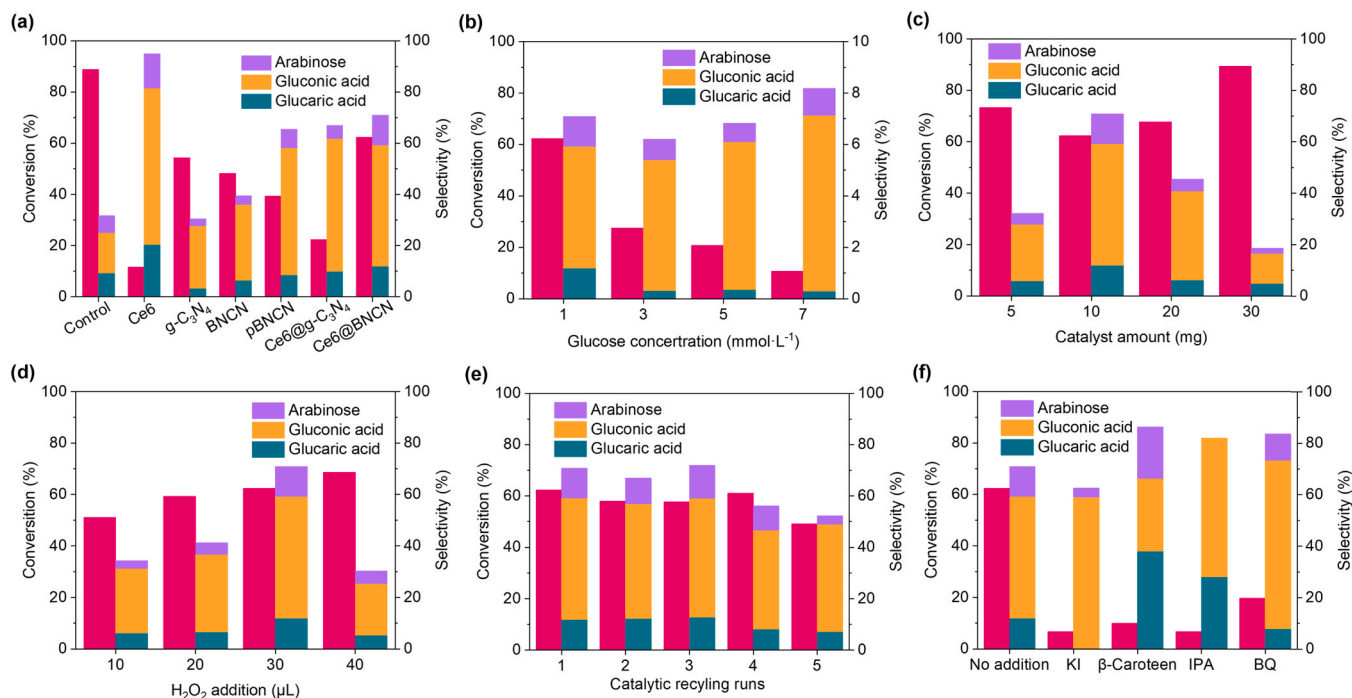
Fig. 3. (a) Photocatalytic oxidation of glucose over different catalysts. Reaction condition: catalyst (10 mg), glucose (1 mmol·L^{-1}, 30 mL), H$_2$O$_2$ (30%, 30 μL), 2 h. Effect of glucose concentration (b), catalyst amount (c) and H$_2$O$_2$ loading (d) on the reaction. (e) Reuse of the Ce6@BNCN catalyst. (f) Effect of scavenger agents on the reaction. Note: left and right column indicate the conversion of glucose and the product selectivities, respectively.

catalyst to various photocatalysts previously tested for glucose oxidation. As shown in Table S3, the catalytic performance of the Ce6@BNCN catalyst far exceed common semiconductor photocatalysts, including ZnO, TiO_2 and C_3N_4 [42,72], suggesting that the combination of semiconductor material with suitable photosensitizer is crucial to promote oxidation reaction and regulate the reaction pathway. In addition, the glucose conversion over the Ce6@BNCN catalyst are obviously higher than other well-designed metal-containing composite photocatalysts with higher or comparable product selectivity [25,43,72–74]. As control, we also attempt to combine several commercially available photosensitizers, including rhodamine B, Cu/tetra (4-carboxyphenyl) porphyrin (TCPP) and Pt/TCPP with g-C_3N_4 using the same synthesis procedure. However, these materials only exhibited limited glucose conversion and product selectivity (Supporting Information, Table S3). The results have demonstrated the superior catalytic performance of the meal-free Ce6@BNCN material for glucose oxidation in all tested catalysts.

3.3. Reasons for excellent catalytic performance

To highlight the mechanism for the improved activity of Ce6@BNCN than other materials, a series of experimental and theoretical studies were carried out. Dramatic PL quenching occurred in the PL emission spectra (Fig. 4a) of BNCN, Ce6@g-C_3N_4 and Ce6@BNCN, among which Ce6@BNCN has lowest PL emission. This result demonstrates that the combination of Ce6 with BNCN considerably inhibits the recombination of photogenerated charge carrier, as is probably due to the strong interaction between photosensitizer and semiconductor.

In electrochemical impedance spectra (EIS) Nyquist plots (Fig. S10), BNCN showed a semicircle diameter that is smaller than g-C_3N_4. This indicates that BNCN has low charge transfer resistance, as is advantageous to electron-hole separation and transfer. Photocurrent time dependence curve is widely employed to examine the charge separation efficiency [75]. BNCN showed obviously higher photocurrent value than

g-C_3N_4. The highest photocurrent value of Ce6@BNCN prove that Ce6@BNCN has best separation efficiency of photogenerated electron and hole.

The ESR analysis (Fig. 4c–f) showed that active species, including ·OH, $O_2^{•−}$ and $^1O_2$ are generated over BNCN and Ce6@BNCN catalyst. Compared with BNCN, the ESR signals of ·OH, $O_2^{•−}$ and $^1O_2$ over Ce6@BNCN composite were all evaluated. In particular, the intensity of ESR signal of $^1O_2$ over Ce6@BNCN composite was significantly greater than that over BNCN. Besides, the low intensity of TEMPO signal for Ce6@BNCN represents that photogenerated electrons generated over Ce6@BNCN are significantly improved in comparison with BNCN.

To confirm the role of different reactive oxygen species, the scavenger experiments (Fig. 3f) were performed using KI, β-carotene, IPA and BQ as scavenger for h^+, $^1O_2$, ·OH and $O_2^{•−}$, respectively. The glucose conversion declined most with the addition of KI, suggesting that h^+ is responsible for the high conversion. The arabinose selectivity declined with the addition of IPA and KI, while it change limitedly with β-carotene and BQ, manifesting that ·OH and h^+ are major active species to induce the formation of arabinose. The selectivity of glucaric acid reduced when adding KI and BQ, while it increased significantly with the addition of β-carotene and IPA, which indicated that $O_2^{•−}$ and h^+ contribute to the generation of glucaric acid. As for gluconic acid, its selectivity reduced significantly with the addition of β-carotene and increased with the addition of KI and BQ. There was little change of gluconic acid selectivity with scavenger IPA, but the glucose conversion decreased significantly. These results indicated that all the four kinds of active species are involved in the generation of gluconic acid from glucose with $^1O_2$ as the most important active specie.

Adsorption of reaction substrates onto the catalyst surface is a primary step in heterogeneous reaction [76,77]. The adsorption behaviors of glucose and organic acids on g-C_3N_4, BNCN and Ce6@BNCN were tested. As shown in Fig. 5a, Ce6@BNCN exhibited slightly higher glucose adsorption capacity than pure g-C_3N_4 and BNCN, as is conducive to the conversion of glucose. DFT calculations also showed that glucose
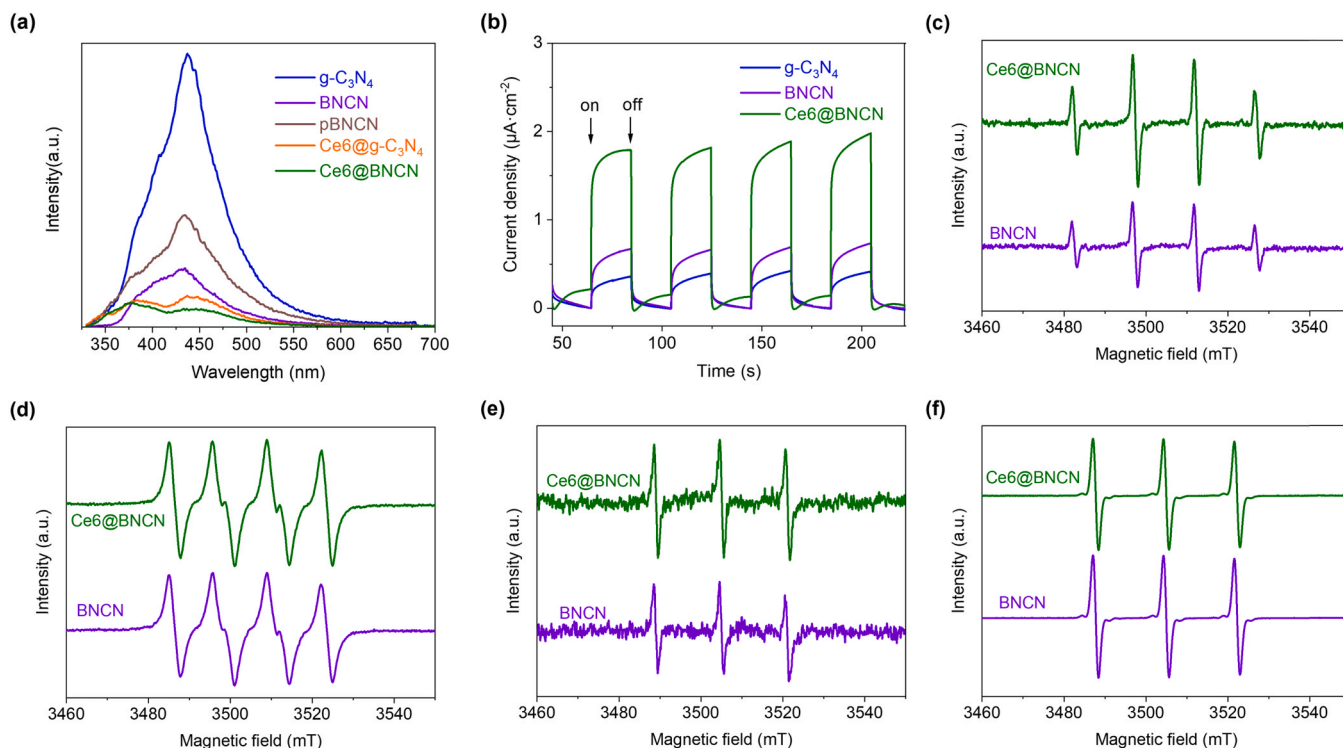
Fig. 4. (a) Steady-state PL emission spectra of g-C_3N_4, BNCN and Ce6@BNCN; (b) Photocurrent time dependence curves of the g-C_3N_4, BNCN and Ce6@BNCN in 0.5 mmol·$L^{−1}$ Na_2SO_4 solution under Xenon lamp irradiation; ESR signals of DMPO-·OH adduct (c) and DMPO-$O_2^{•−}$ adduct (d), and TEMP-$^1O_2$ adduct (e) and TEMPO (f) in the presence of BNCN and Ce6@BNCN composite under Xenon lamp for 10 min.
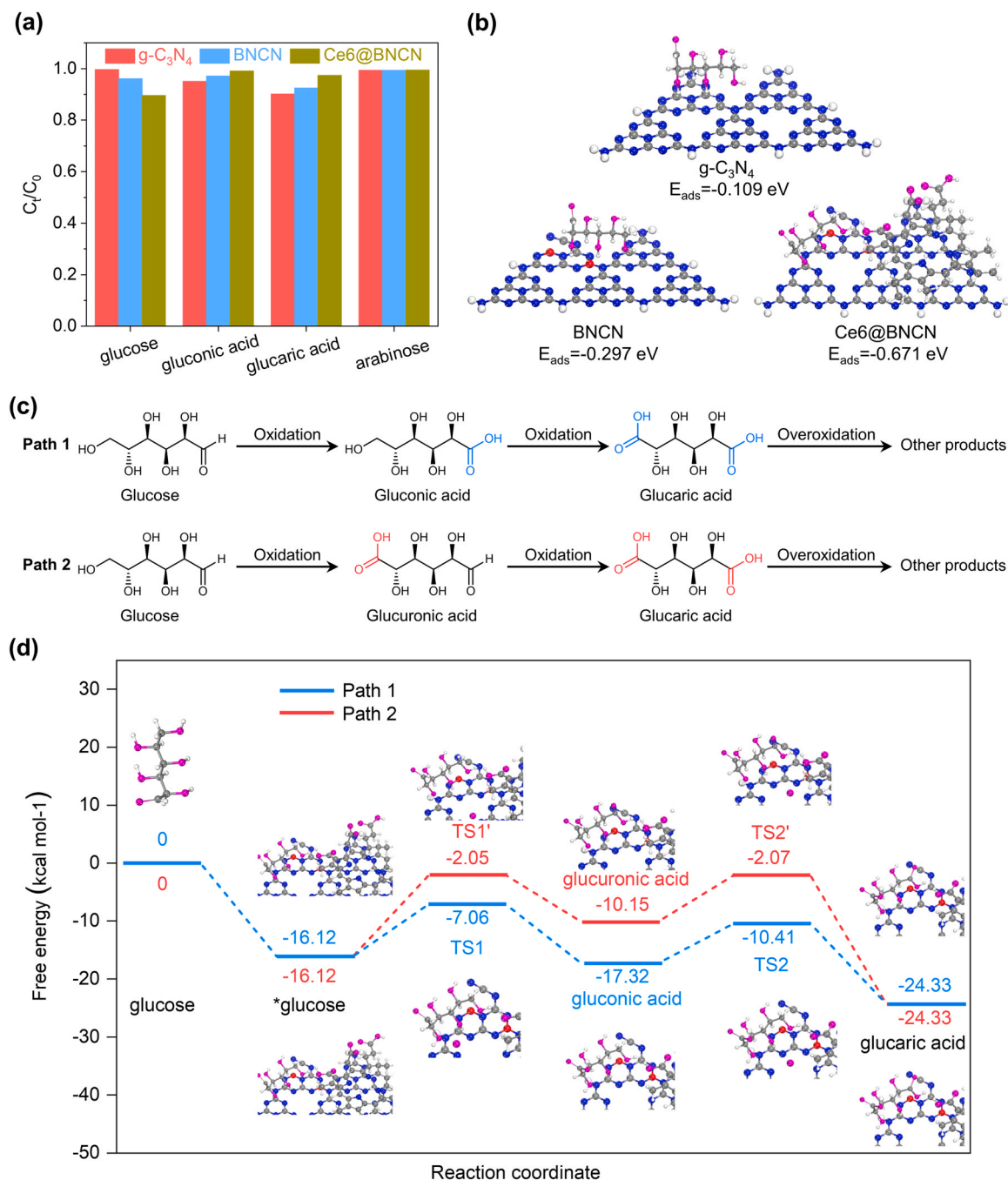
Fig. 5. (a) The adsorption of different substrates on g-C$_3$N$_4$, BNCN and Ce6@BNCN composite. Adsorption condition: material (10 mg), 30 mL of solution with substrate concentration of 1 mmol·L^{-1}. (b) Glucose adsorption energy on g-C$_3$N$_4$, BNCN and Ce6@BNCN. (c) Possible reaction pathway for glucose oxidation to gluconic acid and glucaric acid. (d) DFT calculations for different reaction pathway over Ce6@BNCN.

has the lowest adsorption energy (−0.671 eV) on the surface of Ce6@BNCN (Fig. 5b). Furthermore, the adsorption capacity of oxidation products especially gluconic acid and glucaric acid onto Ce6@BNCN was lower than those onto g-C$_3$N$_4$ and BNCN. These results suggested that the produced organic acids can be readily released from the surface of Ce6@BNCN, as distinct from the other two materials, which is in favor of getting higher selectivity of oxidation products.

In previous reports, the reaction pathway of glucose remains controversial. To verify the two possible reaction pathways (Fig. 5c), the products were detected by LC-MS analysis. The result (Figs. S11–S14) indicated the two possible reaction pathways both occurred in the present photocatalytic system, as is different from the conclusion on the iron thioporphyrazine/SnO$_2$ catalyst [32]. Meanwhile, LC-MS analysis

also proved that both gluconic acid and glucuronic acid can be converted to glucaric acid (Figs. S15 and 16) by the catalytic system. DFT calculations were further conducted to elucidate the favorable reaction pathway. As shown in Fig. 5d, the energy barrier (9.06 kcal mol^{-1}) for the conversion of glucose to gluconic acid over the Ce6@BNCN catalyst is significantly lower than the conversion of glucose to glucuronic acid (14.07 kcal mol^{-1}), indicating the former reaction pathway is easier to occur in the catalytic system. By contrast, the energy barrier (6.91 kcal mol^{-1}) for the conversion of gluconic acid to glucaric acid is lower than that (8.08 kcal mol^{-1}) for the conversion of gluconic acid to glucuronic acid. The similar energy barrier suggests that the catalytic system can convert gluconic acid and glucuronic acid into glucaric acid in parallel. Therefore, the combined experimental results and DFT

calculations indicate that the oxidation of glucose to gluconic acid and glucaric acid is proceeded mainly via the Path 1. Besides, the energy barrier (20.9 and 12.03 kcal mol^{-1}, respectively) for the conversion of glucose to gluconic acid over the g-C$_3$N$_4$ and BNCN catalyst are significantly higher than that over the Ce6 @BNCN catalyst (Fig. S17), as is in good accordance with the activity trends. In the present work, the inhibition of overoxidation and mineralization is achieved through multiple parameters, including the improved generation of ^{1}O$_2$, the enhanced desorption of organic acids from catalyst as well as the control of reaction conditions. However, it's still difficult to completely avoid overoxidation and mineralization. The design of photocatalyst which could selectively generate target active radicals is still on the way.

4. Conclusion

We have successfully synthesized Ce6@BNCN composite as highly effective metal-free photocatalyst for the selective oxidation of glucose to high-value products. We show that introducing nitrogen defects into g-C$_3$N$_4$ as well as combining BNCN with Ce6 could improve the optical absorption property, boost the separation efficiency of photon-generated carriers and eventually enhance the generation of reactive oxygen species. The photocatalytic oxidation of glucose over Ce6@BNCN with H$_2$O$_2$ as oxidant afforded high glucose conversion with excellent selectivity of gluconic acid, glucaric acid and arabinose under optimized condition, surpassing g-C$_3$N$_4$, Ce6 and many previously reported photocatalytic materials. The superior performance was attributed to the improved light response and photogenerated carriers separation efficiency in Ce6@BNCN, owing to the interaction between Ce6 and BNCN. DFT calculations also confirm that selectively oxidizing glucose toward gluconic acid and glucaric acid with Ce6@BNCN catalyst is thermodynamically easier to occur than other catalysts. Besides, both adsorption experiment and DFT calculation proved that Ce6@BNCN has higher glucose adsorption capacity but lower gluconic acid, glucaric acid adsorption capacity, as another important factor for the enhanced catalytic performance.

CRediT authorship contribution statement

Xinyu Bai: Data curation, Writing – original draft. **Qidong Hou:** Conceptualization, Writing – review & editing, Supervision. **Hengli Qian:** Methodology. **Yifan Nie:** Methodology. **Tianliang Xia:** Investigation. **Ruite Lai:** Investigation. **Guanjie Yu:** Investigation. **Mian Laiq Ur Rehman:** Methodology. **Haijiao Xie:** Software. **Meiting Ju:** Supervision.

Declaration of Competing Interest

The authors declare that they have no known competing financial interests or personal relationships that could have appeared to influence the work reported in this paper.

Acknowledgements

Appendix A. Supporting information

Supplementary data associated with this article can be found in the online version at doi:10.1016/j.apcatb.2021.120895.

References

[1] Z. Zhang, J. Song, B. Han, Catalytic transformation of lignocellulose into chemicals and fuel products in ionic liquids, Chem. Rev. 117 (2016) 6834–6880.

[2] L. Hu, Z. Wu, Y. Jiang, A. He, J. Xu, Recent advances in catalytic and autocatalytic production of biomass-derived 5-hydroxymethylfurfural, Renew. Sustain. Energy Rev. 134 (2020), 110317.

[3] X. Wu, S. Xie, H. Zhang, Q. Zhang, B. Sels, Y. Wang, Metal sulfide photocatalysts for lignocellulose valorization, Adv. Mater. (2021), 2007129.

[4] X. Wu, N. Luo, S. Xie, H. Zhang, Y. Wang, Photocatalytic transformations of lignocellulosic biomass into chemicals, Chem. Soc. Rev. 49 (2020) 6198–6223.

[5] X. Yuan, P.D. Dissanayake, B. Gao, W.J. Liu, S.O. Yong, Review on upgrading organic waste to value-added carbon materials for energy and environmental applications, J. Environ. Manag. 296 (2021), 113128.

[6] W. Liu, L. Dang, Z. Xu, H.Q. Yu, S. Jin, G.W. Huber, Electrochemical oxidation of 5-hydroxymethylfurfural with NiFe layered double hydroxide (LDH) nanosheet catalysts, ACS Catal. 8 (2018) 5533–5541.

[7] J. Ma, K. Liu, X. Yang, D. Jin, Y. Li, G. Jiao, J. Zhou, R. Sun, Recent advances and challenges in photoreforming of biomass-derived feedstocks into hydrogen, biofuels, or chemicals by using functional carbon nitride photocatalysts, ChemSusChem 14 (2021) 1–21.

[8] V. Choudhary, S.H. Mushrif, C. Ho, A. Anderko, D.G. Vlachos, Insights into the interplay of lewis and brnsted acid catalysts in glucose and fructose conversion to 5-(hydroxymethyl)furfural and levulinic acid in aqueous media, J. Am. Chem. Soc. 135 (2013) 3997–4006.

[9] M. Chidambaram, A.T. Bell, A two-step approach for the catalytic conversion of glucose to 2,5-dimethylfuran in ionic liquids, Green Chem. 12 (2010) 1253–1262.

[10] W.J. Liu, Z. Xu, D. Zhao, X.Q. Pan, H.Q. Yu, Efficient electrochemical production of glucaric acid and H$_2$ via glucose electrolysis, Nat. Commun. 11 (2020) 1–11.

[11] J.C. Colmenares, A. Magdziarz, A. Bielejewska, High-value chemicals obtained from selective photo-oxidation of glucose in the presence of nanostructured titanium photocatalysts, Bioresour. Technol. 102 (2011) 11254–11257.

[12] J.C. Colmenares, A. Magdziarz, K. Kurzydlowski, J. Grzonka, O. Chernyayeva, D. Lisovytskiy, Low-temperature ultrasound-promoted synthesis of Cr–TiO$_2$-supported photocatalysts for valorization of glucose and phenol degradation from liquid phase, Appl. Catal. B Environ. 134 (2013) 136–144.

[13] C. Juan, Agnieszka Colmenares, Olga Magdziarz, Dmytro Chernyayeva, Krzysztof Lisovytskiy, Sonication-assisted low-temperature routes for the synthesis of supported Fe-TiO$_2$ econanomaterials: partial photooxidation of glucose and phenol aqueous degradation, ChemCatChem 5 (2013) 2270–2277.

[14] B. Jin, G. Yao, X. Wang, K. Ding, F. Jin, Photocatalytic oxidation of glucose into formate on nano TiO$_2$ catalyst, ACS Sustain. Chem. Eng. 5 (2017) 6377–6381.

[15] A. Liu, Z. Huang, X. Wang, Efficient Oxidation of Glucose into Gluconic Acid Catalyzed by Oxygen-Rich Carbon Supported Pd Under Room Temperature and Atmospheric Pressure, Catal. Lett. 148 (2018) 2019–2029.

[16] X. Jin, M. Zhao, M. Vora, J. Shen, C. Zeng, W. Yan, P.S. Thapa, B. Subramaniam, R. V. Chaudhari, Synergistic effects of bimetallic PtPd/TiO$_2$ nanocatalysts in oxidation of glucose to glucaric acid: structure dependent activity and selectivity, Ind. Eng. Chem. Res. 55 (2016) 2932–2945.

[17] W. Deng, Q. Zhang, W. Ye, Catalytic transformations of cellulose and cellulose-derived carbohydrates into organic acids, Catal. Today 234 (2014) 31–41.

[18] A. Corma, S. Iborra, A. Velty, Chemical routes for the transformation of biomass into chemicals, Chem. Rev. 107 (2007) 2411–2502.

[19] Sumitra Ramachandran, Pierre Fontanille, Ashok Pandey, Christian Larroche, Gluconic acid: properties, applications and microbial production, Food Technol. Biotechnol. 44 (2006) 185–195.

[20] Basudeb Saha, Vlachos, G. Dionisios, Jechan Lee, Pt catalysts for efficient aerobic oxidation of glucose to glucaric acid in water, Green Chem. 18 (2016) 3815–3822.

[21] J. Bozell, G. Petersen, Technology development for the production of biobased products from biorefinery carbohydrates-the US Department of Energy's "Top 10" revisited, Green Chem. 12 (2010) 539–554.

[22] H.M. Qin, Y.U. Zong-Yuan, R.B. Rong, Advances in L-arabinose research, Chem. Bioeng. 2 (2006).

[23] Z. Xu, S. Li, X. Feng, J. Liang, H. Xu, L-Arabinose isomerase and its use for biotechnological production of rare sugars, Appl. Microbiol. Biotechnol. 98 (2014) 8869–8878.

[24] M. Yamaguchi, T. Mukaiyama, The stereoselective synthesis of D- and L-ribose, Chem. Lett. 7 (1981) 1005–1008.

[25] R. Chen, C. Yang, Q. Zhang, B. Zhang, K. Deng, Visible-light-driven selective oxidation of glucose in water with H-ZSM-5 zeolite supported biomimetic photocatalyst, J. Catal. 374 (2019) 297–305.

[26] Q. Zhang, X. Xiang, Y. Ge, C. Yang, B. Zhang, K. Deng, Selectivity enhancement in the g-C$_3$N$_4$ -catalyzed conversion of glucose to gluconic acid and glucaric acid by modification of cobalt thioporphyrazine, J. Catal. 388 (2020) 11–19.

[27] N. Chen, J. Wang, Y. Zhao, Y. Deng, Metabolic engineering of Saccharomyces cerevisiae for efficient production of glucaric acid at high titer, Microb. Cell Fact. 17 (2018) 1–11.

[28] S. Solmi, C. Morreale, F. Ospitali, S. Agnoli, F. Cavani, Oxidation of d-Glucose to glucaric acid using Au/C catalysts, ChemCatChem 9 (2017) 2797–2806.

[29] E. Derrien, M. Mounguengui-Diallo, N. Perret, P. Marion, C. Pinel, M. Besson, Aerobic oxidation of glucose to glucaric acid under alkaline-free conditions: Au-based bimetallic catalysts and the effect of residues in a hemicellulose hydrolysate, Ind. Eng. Chem. Res. 56 (2017) 13175–13189.

[30] T.N. Smith, K. Hash, C.L. Davey, H. Mills, H. Williams, D.E. Kiely, Modifications in the nitric acid oxidation of d -glucose, Carbohydr. Res. 350 (2012) 6–13.

[31] X. Shuai, P. Zhou, Z. Zhang, C. Yang, B. Zhang, K. Deng, S.E. Bottle, H. Zhu, Selective oxidation of 5-hydroxymethylfurfural to 2,5-furandicarboxylic acid using O_2 and a photocatalyst of Co-thioporphyrazine bonded to g-C_3N_4, J. Am. Chem. Soc. 139 (2017) 14775–14782.

[32] Q. Zhang, Y. Ge, C. Yang, B. Zhang, K. Deng, Enhanced photocatalytic performance for oxidation of glucose to value-added organic acids in water using iron thioporphyrazine modified SnO_2, Green Chem. 21 (2019) 5019–5029.

[33] J. Ma, D. Jin, Y. Li, D. Xiao, G. Jiao, Q. Liu, Y. Guo, L. Xiao, X. Chen, X. Li, J. Zhou, R. Sun, Photocatalytic conversion of biomass-based monosaccharides to lactic acid by ultrathin porous oxygen doped carbon nitride, Appl. Catal. B Environ. 283 (2021), 119520.

[34] J. Ma, Y. Li, D. Jin, X. Yang, G. Jiao, K. Liu, S. Sun, J. Zhou, R. Sun, Reasonable regulation of carbon/nitride ratio in carbon nitride for efficient photocatalytic reforming of biomass-derived feedstocks to lactic acid, Appl. Catal. B Environ. 299 (2021) 120698.

[35] Y. Li, J. Ma, D. Jin, G. Jiao, X. Yang, K. Liu, J. Zhou, R. Sun, Copper oxide functionalized chitosan hybrid hydrogels for highly efficient photocatalytic-reforming of biomass-based monosaccharides to lactic acid, Appl. Catal. B Environ. 291 (2021), 120123.

[36] J. Ma, Y. Li, D. Jin, Z. Ali, G. Jiao, J. Zhang, S. Wang, R. Sun, Functional B@mCN-assisted photocatalytic oxidation of biomass-derived pentoses and hexoses to lactic acid, Green Chem. 22 (2020) 6384–6392.

[37] J. Ma, D. Jin, X. Yang, S. Sun, J. Zhou, R. Sun, Phosphorus-doped carbon nitride with grafted sulfonic acid groups for efficient photocatalytic synthesis of xylonic acid, Green Chem. 23 (2021) 4150–4160.

[38] M. Bellardita, E.I. García-López, G. Marcìa, B. Megnab, F.R. Pomilla, L. Palmisano, Photocatalytic conversion of glucose in aqueous suspensions of heteropolyacid–TiO_2 composites, RSC Adv. 5 (2015) 59037–59047.

[39] M. Bellardita, E.I. García-López, G. Marcì, L. Palmisano, Photocatalytic formation of H_2 and value-added chemicals in aqueous glucose (Pt)-TiO_2 suspension, Int. J. Hydrog. Energy 41 (2016) 5934–5947.

[40] Baowen Zhou, Jinliang Song, Zhanrong Zhang, Zhiwei Jiang, Han Pei, Highly selective photocatalytic oxidation of biomass-derived chemicals to carboxyl compounds over Au/TiO_2, Green Chem. 19 (2017) 1075–1081.

[41] M. Omri, F. Sauvage, Y. Busby, M. Becuwe, G. Pourceau, A. Wadouachi, Gold catalysis and photoactivation: a fast and selectiveprocedure for the oxidation of free sugars, ACS Catal. 8 (2018) 1635–1639.

[42] D. Vies, E. Thomas, Gonzalez-Yanez, O. Edgar, Lopez-Sanchez, A. Jose, Da, Visible light selective photocatalytic conversion of glucose by TiO_2, Appl. Catal. B Environ. 202 (2017) 281–288.

[43] Q. Zhang, X. Xiang, Y. Ge, C. Yang, B. Zhang, K. Deng, Selectivity enhancement in the g-C_3N_4-catalyzed conversion of glucose to gluconic acid and glucaric acid by modification of cobalt thioporphyrazine, J. Catal. 388 (2020) 11–19.

[44] Y. Liu, A. Mh, G.A. Rui, A. Zf, S. Kang, M.B. Zhen, M.D. C, W.D. Wang, L. Cui, Ultrastable metal-free near-infrared-driven photocatalysts for H_2 production based on protonated 2D g-C_3N_4 sensitized with Chlorin e6, Appl. Catal. B Environ, 260, 118137.

[45] J. Chen, D. Zhao, Z. Diao, M. Wang, S. Shen, Ferrites boosting photocatalytic hydrogen evolution over graphitic carbon nitride: a case study of (Co, Ni) Fe_2O_4 modification, Sci. Bull., 61, 292–301.

[46] J. Chen, D. Zhao, Z. Diao, M. Wang, L. Guo, S. Shen, Bifunctional modification of graphitic carbon nitride with $MgFe_2O_4$ for enhanced photocatalytic hydrogen generation, ACS Appl. Mater. Interfaces 7 (2015) 18843–18848.

[47] D. Zhao, C. Dong, B. Wang, C. Chen, S. Shen, Synergy of dopants and defects in graphitic carbon nitride with exceptionally modulated band structures for efficient photocatalytic oxygen evolution, Adv. Mater. 31 (2019), 1903545.

[48] L. Wang, X. Zheng, L. Chen, Y. Xiong, H. Xu, Van der Waals heterostructures comprised of ultrathin polymer nanosheets for efficient Z-scheme overall water splitting, Angew. Chem. 130 (2018) 3512–3516.

[49] B.J. Delley, From molecules to solids with the $DMol_3$ approach, J. Chem. Phys. 113 (2000) 7756–7764.

[50] J.P. Perdew, K. Burke, M. Ernzerhof, Generalized gradient approximation made simple, Phys. Rev. Lett. 77 (1998) 3865–3868.

[51] B. Delley, Hardness conserving semilocal pseudopotentials, Phys. Rev. B Condens. Matter 66 (2002), 155125.

[52] S. Grimme, Semiempirical GGA-type density functional constructed with a long-range dispersion correction, J. Comput. Chem. 27 (2010) 1787–1799.

[53] Ye Meng-Yang, Zhao Zhi-Hao, Hu Zhuo-Feng, Liu Le-Quan, 0D/2D heterojunctions of vanadate quantum dots/graphitic carbon nitride nanosheets for enhanced visible-light-driven photocatalysis, Angew. Chem. Int. Ed. 56 (2017) 8407–8411.

[54] Y. Li, Z. Wang, T. Xia, H. Ju, K. Zhang, R. Long, Q. Xu, C. Wang, L. Song, J. Zhu, Implementing metal-to-ligand charge transfer in organic semiconductor for improved visible-near-infrared photocatalysis, Adv. Mater. 28 (2016) 6959–6965.

[55] M. Chen, Y. Zhang, L. Cui, Z. Cao, Y. Wang, W. Zhang, Y. Zheng, D. Sun, L. Zheng, S. Kang, D. Zhang, Protonated 2D carbon nitride sensitized with Ce6 as a smart metal-free nanoplatform for boosted acute multimodal photo-sono tumor inactivation and long-term cancer immunotherapy, Chem. Eng. J. 422 (2021), 130089.

[56] D. Sun, Z. Zhang, M. Chen, Y. Zhang, J. Amagat, S. Kang, Y. Zheng, B. Hu, M. Chen, Co-immobilization of Ce6 sono/photosensitizer and protonated graphitic carbon nitride on pcl/gelation fibrous scaffolds for combined sono-photodynamic cancer therapy, ACS Appl. Mater. Interfaces 12 (2020) 40728–40739.

[57] Dong Xi-Yan, Zhang Mei, Pei Ru-Bo, Wang Qian, Dong-Hui, A crystalline copper(II) coordination polymer for the efficient visible-light-driven generation of hydrogen, Angew. Chem. 55 (2016) 2073–2077.

[58] X. Cai, M. Zhu, O.A. Elbanna, M. Fujitsuka, S. Kim, L. Mao, J. Zhang, T. Majima, Au nanorods photosensitized $La_2Ti_2O_7$ nanosteps: successive surface heterojunctions boosting visible to near-infrared photocatalytic H_2 evolution, ACS Catal. 8 (2017) 122–131.

[59] W. Zhen, M. Liu, Z. Zhang, W. Yao, H. Tan, Y. Zhu, Efficient visible-light-driven selective oxygen reduction to hydrogen peroxide by oxygen-enriched graphitic carbon nitride polymers, Energy Environ. Sci. 11 (2018) 2581–2589.

[60] R. Sprick, S. Bonillo, B. Clowes, R. Guiglion, P. Brownbill, Visible-light-driven hydrogen evolution using planarized conjugated polymer photocatalysts, Angew. Chem. 55 (2018) 1792–1796.

[61] X. Peng, T. Peng, L. Yu, R. Li, L. Zhen, Visible/near-infrared-light-induced H_2 production over g-C_3N_4 co-sensitized by organic dye and zinc phthalocyanine derivative, ACS Catal. 5 (2015) 504–510.

[62] H. Yu, R. Shi, Y. Zhao, T. Bian, Y. Zhao, C. Zhou, G.I.N. Waterhouse, L.-Z. Wu, C.-H. Tung, T. Zhang, Alkali-assisted synthesis of nitrogen deficient graphitic carbon nitride with tunable band structures for efficient visible-light-driven hydrogen evolution, Adv. Mater. 29 (2017), 1605148.

[63] Yu Huijun, Shi Run, Zhao Yunxuan, Bian Tong, Zhao Yufei, Photocatalysis: alkali-assisted synthesis of nitrogen deficient graphitic carbon nitride with tunable band structures for efficient visible-light-driven hydrogen evolution, Adv. Mater. 29 (2017), 605148.

[64] X. Zhang, L. Yu, C. Zhuang, T. Peng, X. Li, Highly asymmetric phthalocyanine as a sensitizer of graphitic carbon nitride for extremely efficient photocatalytic h2 production under near-infrared light, ACS Catal. 4 (2014) 162–170.

[65] Mingshan, Osakada, Yasuko, Sooyeon, Fujitsuka, Mamoru, Majima, Tetsuro, Black phosphorus: a promising two dimensional visible and near-infrared-activated photocatalyst for hydrogen evolution, Appl. Catal. B Environ., 217, 285–292.

[66] S. Liu, H. Sun, H.M. Ang, M.O. Tade, S. Wang, Integrated oxygen-doping and dye sensitization of graphitic carbon nitride for enhanced visible light photodegradation, J. Colloid Interf. Sci. 476 (2016) 193–199.

[67] H. Yu, R. Shi, Y. Zhao, T. Bian, Y. Zhao, C. Zhou, G.I.N. Waterhouse, L.-Z. Wu, C.-H. Tung, T. Zhang, Alkali-assisted synthesis of nitrogen deficient graphitic carbon nitride with tunable band structures for efficient visible-light-driven hydrogen evolution, Adv. Mater. 29 (2017), 1605148.

[68] M. Zhu, S. Kim, M. Liang, M. Fujitsuka, J. Zhang, X. Wang, T. Majima, Metal-free photocatalyst for H_2 evolution in visible to near-infrared region: black phosphorus/graphitic carbon nitride, J. Am. Chem. Soc. 139 (2017) 13234–13242.

[69] W. Lei, R.F. Erán, Z. Lei, D. Fernandes, H. Tian, Organic polymer dots as photocatalysts for visible light-driven hydrogen generation, Angew. Chem. 128 (2016) 12494–12498.

[70] W.W. A, G.L. A, T.A. A, D.K.L.C. B, J.C.Y. B, P.K.W. C, Photocatalytic hydrogen evolution and bacterial inactivation utilizing sonochemical-synthesized g-C_3N_4/red phosphorus hybrid nanosheets as a wide-spectral-responsive photocatalyst: the role of type I band alignment, Appl. Catal. B Environ. 238 (2018) 126–135.

[71] W. Wang, T. An, G. Li, D. Xia, H. Zhao, J.C. Yu, P.K. Wong, Earth-abundant Ni_2P/g-C_3N_4 lamellar nanohydrids for enhanced photocatalytic hydrogen evolution and bacterial inactivation under visible light irradiation, Appl. Catal. B Environ. 217 (2017) 570–580.

[72] Q. Zhang, Y. Ge, C. Yang, B. Zhang, K.D. En G, Enhanced photocatalytic performance for oxidation of glucose to value-added organic acids in water using iron thioporphyrazine modified SnO_2, Green Chem. 21 (2019) 5019–5029.

[73] Q. Zhang, C. Yang, B. Zhang, K. Deng, Cobalt porphyrazine supported on SnO_2 with oxygen vacancies for boosting photocatalytic aerobic oxidation of glucose to organic acids in an aqueous medium, ACS Sustain. Chem. Eng. 9 (2021) 2057–2066.

[74] J. Yin, Q. Zhang, C. Yang, B. Zhang, K. Deng, Highly selective oxidation of glucose to gluconic acid and glucaric acid in water catalyzed by an efficient synergistic photocatalytic system, Catal. Sci. Technol. 10 (2020) 2231–2241.

[75] F.T. Li, S.J. Liu, Y.B. Xue, X.J. Wang, D. Zhao, Structure modification function of g-C_3N_4 for Al_2O_3 in the in situ hydrothermal process for enhanced photocatalytic activity, Chemistry 21 (2015) 10149–10159.

[76] Y. Ying, J.C. Yu, C.Y. Chan, Y.K. Che, J.C. Zhao, L. Ding, W.K. Ge, P.K. Wong, Enhancement of adsorption and photocatalytic activity of TiO_2 by using carbon nanotubes for the treatment of azo dye, Appl. Catal. B Environ. 61 (2005) 1–11.

[77] C.H. Liang, F.B. Li, C.S. Liu, J.L. Lü, X.G. Wang, The enhancement of adsorption and photocatalytic activity of rare earth ions doped TiO_2 for the degradation of Orange, Dyes Pigments 76 (2008) 477–484.